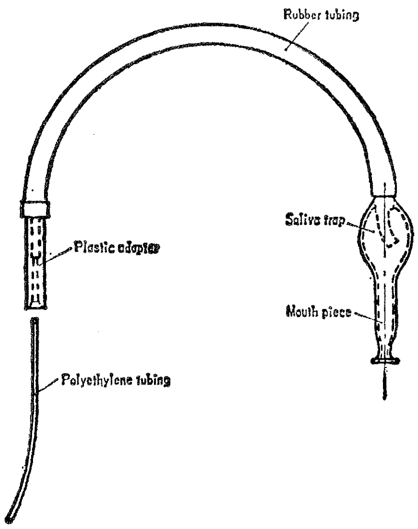

Fig. 2. Oral suction device.

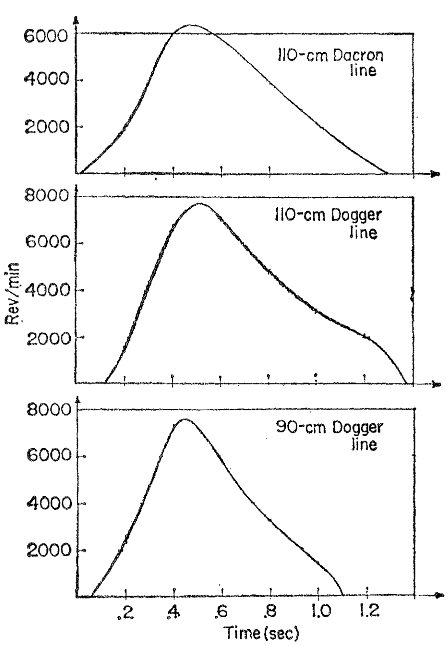

Fig. 3. Test speeds attained with two lengths of two different types of cord.

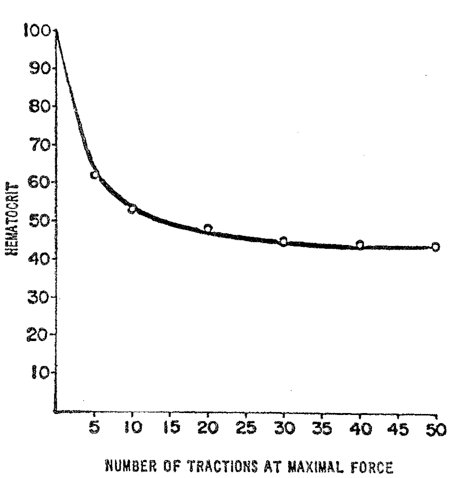

Fig. 4. Hematocrit values obtained with microcentrifuge.

attachment to any solid object; the other four pierce a wooden handle, beyond which they are knotted.

Inside and outside diameters, respectively, of the tubing used (*4*) are 0.76 or 0.86 mm and 1.22 or 1.27 mm. Any similar good polyethylene tubing would serve. The tubing must be heparinized by (i) blowing through the coil 1-percent heparine solution in saline, (ii) blowing air through the coil, and (iii) leaving the tubing to dry.

A suction device ("filler") for filling and emptying the polyethylene tubes is shown in Fig. 2. Other accessories are a metal rod for aiding insertion and removal of the tubes in and from the disc, small forceps, and scissors.

A length of tubing, inserted in the plastic adaptor of the filler (Fig. 2), is sucked almost full of the sample. Doubled into U-form, the filled tubing is then inserted in one of the disc channels, doubled-end first, from a midpoint of the disc. The procedure then is to grasp the handle, tauten the cords, and manually rotate the disc (located at the center of the cords); release the disc, allowing it to spin, and then accelerate the spin by alternately tensing and slackening the cords; spin the disc ten or more times at top speed until separation of the sample is visibly complete; and withdraw the tubing and separate the separated components of the sample by cutting the tubing with scissors. A gentle blow through the filler deposits a component on glass slides.

A disc was tested electronically with three cords of different length or construction; the results appear in Fig. 3. With traction of 19 to 20 kg, the disc repeatedly exceeded 10,000 rev/min, radial acceleration exceeding 8400*g*. The speed of the disc is great enough to seriously injure anyone contacting it.

A test determination for (female) hematocrit (Fig. 4) yielded a result of 44 percent; the normal range is 35.8 to 45.4 percent, with a standard deviation of 2.3 percent (*5*). The constant change in direction of rotation, with accompanying deceleration and acceleration, has no practical effect.

Among other uses, the centrifuge serves to obtain plasma for immunoelectrophoresis and flocculation and agglutination tests and for determination of plasma cholinesterase and total solids (refractometrically). Blood parasites may be concentrated in the red-cell layer. The centrifuge may be useful in other biological sciences as well as in medical research.

Bo Holmstedt
Department of Toxicology, Swedish Medical Research Council, Karolinska Institutet, Stockholm 60

References and Notes

1. C. G. Hedén and E. Meyer, *Acta Pathol. Microbiol. Scand.* **55**, 447 (1962).
2. S. Sailer and H. Braunsteiner, *Klin. Wochschr.* **37**, 986 (1959). The Acholest papers are available from Österreichisches Stickstoffwerke Aktiengesellschaft, Linz/Donau, St. Peter 224; the method has been recently modified to include a wet standard. I thank Dr. R. Kilches for sample and information.
3. Yarns No. 250/10 or 250/12 made by Nils Wennerström, Lidingö 1, Sweden. Corresponding English cotton numbers are 12/15 and 12/18, respectively; the latter is preferable.
4. Tubing made by Clay-Adams, Inc., 141 East 25 Street, New York 10010.
5. *Documenta Geigy, Series chirurgica* "Scientific tables" (1956), p. 335.
6. Development supported by WHO; a detailed report is available as WHO/Mal/486.65. The centrifuge is being manufactured by Ingenjörsfirman Instrumenttjänst, Box 57, Sundbyberg 1, Sweden. I thank Pehr Clementz, Gösta Lundgren, and Lars Sjöstedt for assistance.

18 March 1965

Lidar Observation of Cloud

Abstract. *Lidar (from "light detection and ranging") is the optical counterpart of meteorological radar. At optical wavelengths, very much smaller atmospheric particles can be detected than at microwave wavelengths. With a laser power source, a transmitter uses a lens system to beam very intense pulses of monochromatic light of extremely short duration. Light backscattered by the atmosphere is collected in a receiver system that is essentially a telescope coaligned with the transmitter, and a narrow-pass filter allows only light of the transmitted frequency to be detected by a photomultiplier. Data are presented on an oscilloscope as a trace of signal intensity versus range (the A-scope of radar practice) and photographed.*

Since August 1963 an experimental program at Stanford Research Institute has used single-shot, giant-pulse ruby lasers in certain systems whose specifications appear in Table 1. In these systems, peak powers of many megawatts are attained in pulses having an equivalent length of some 4 m. The coherence and monochromaticity of the laser-generated light make it possible to achieve very well-collimated beams and also to reduce interference from solar energy by the use of filters in daylight operation. The current, mobile version is illustrated in Fig. 1.

Many interesting and significant observations of meteorological phenomena have been made, including observations of "clear air" (*1*, *2*). My purpose in this report is to describe specifically the use and potential of lidar (*1*) in observing clouds.

The distance at which clouds can be detected depends upon the density of the clouds, the transmissivity of the atmosphere, and the amount of solar illumination scattered by the atmosphere—all in conjunction with the performance of the system in use. As a general rule, the lidars used in our experiments could detect all cloud visible to the eye within, say, 45 deg of the zenith by day, and could penetrate through thin cloud layers. Under very clear conditions, clouds can be detected at much lower angles; at night, when solar-energy noise is absent, all detection is greatly enhanced.

Lidar observations of cloud may be in various forms. Cloud-base height can be measured in the case of both layered and isolated clouds; observations can be made obliquely, and upper-cloud data can be obtained by making observations through gaps in lower-cloud cover, even when the gap is not overhead. Vertical development of distant clouds may be assessed from slant range and elevation of the cloud tops. The gradient of cloud density at the surface of clouds may be inferred from the nature of the lidar "echo," particularly for cloud bases. A rapid transition from clear air to dense cloud is marked by a clean-cut echo profile, with rapid attenuation of the lidar signal. Diffuse cloud bases show prolonged traces, but there is little difficulty in recognizing the cloud boundary, and height measurements can be made with precision in conditions where, to the eye, the cloud base is completely indeterminate. This is es-

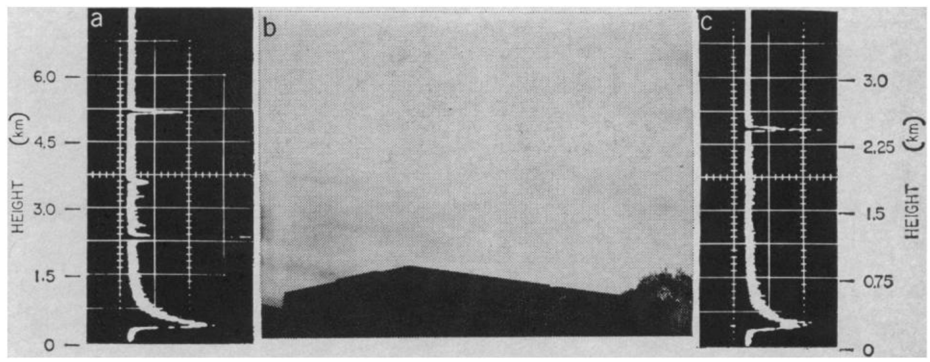

Fig. 2. Altostratus clouds and cloud observations, 28 October 1964. (*a*) Vertical lidar observation at 1107 PST; elevation, 90 deg. (*b*) Sky at 1150 PST. (*c*) Lidar observation in light rain (reduced gain) at 1427 PST; elevation, 30 deg; height of cloud base, 2.4 km, seen at a slant range of 4.8 km.

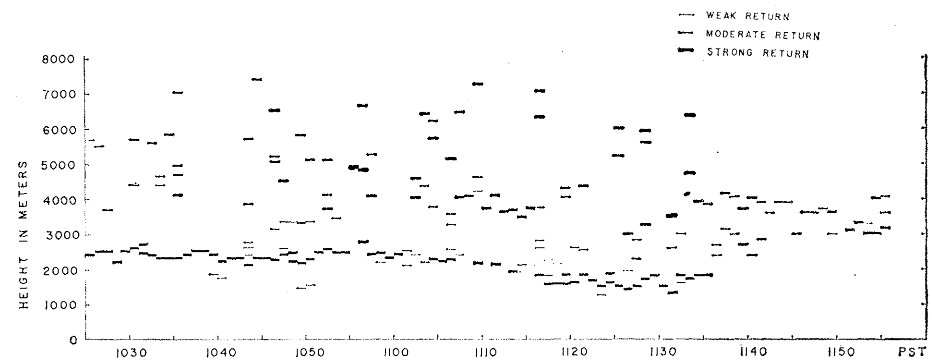

Fig. 3. Altostratus cloud, 28 October 1964. Time : height section constructed from series of vertical lidar observations made at intervals of 1 minute.

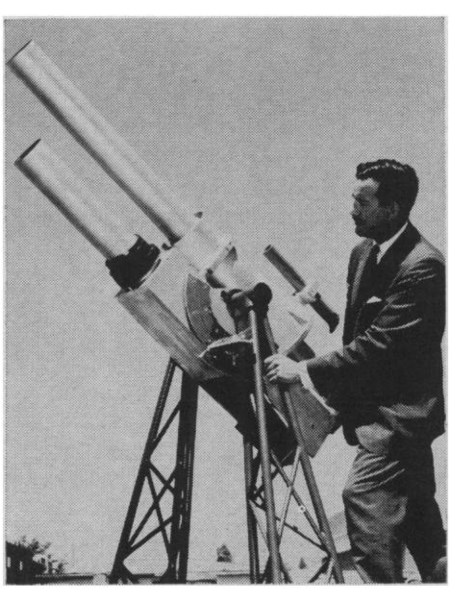

Fig. 1. Experimental mobile lidar, Mark I 1964.

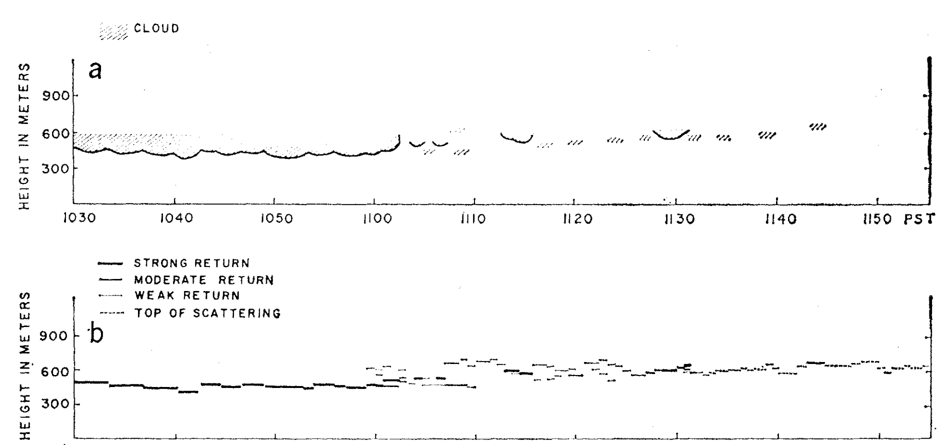

Fig. 4. Low stratus cloud, 29 September 1964. (*a*) Record of visual observations made through the lidar's aiming telescope coincidentally with each lidar shot. (*b*) Time : height section constructed from vertical lidar observations made at intervals varying from 40 seconds to 2 minutes.

pecially noteworthy at times when rain or drizzle is falling from nimbostratus. The following specific examples illustrate the general capabilities of lidar in observing cloud.

Multiple-layered medium cloud. In the forenoon of 28 October 1964 the sky was overcast; a fairly continuous sheet of altostratus lowered steadily until it broke up as light rain fell at about 1140 PST. A higher layer of altostratus, which previously had been visible through gaps in the lower layer, was then seen to cover the sky, which about noon had the appearance seen in Fig. 2*b*. Figure 2*a* shows one sample out of a continuous series of observations made with a vertically pointing lidar at 1-minute intervals. Figure 3 is a profile made from this series. In the afternoon, during continuous light-to-moderate rain, further measurements were made of the cloud base; because the experimental equipment used was not designed for operation in rain, it was possible to make shots only at 30-deg elevation. Figure 2*c* shows a typical result, with the cloud base at an altitude of 2400 m. It is worth noting that visual estimates of cloud base by experienced meteorologists on this and other days were often considerably in error, particularly when the sky was amorphous in appearance.

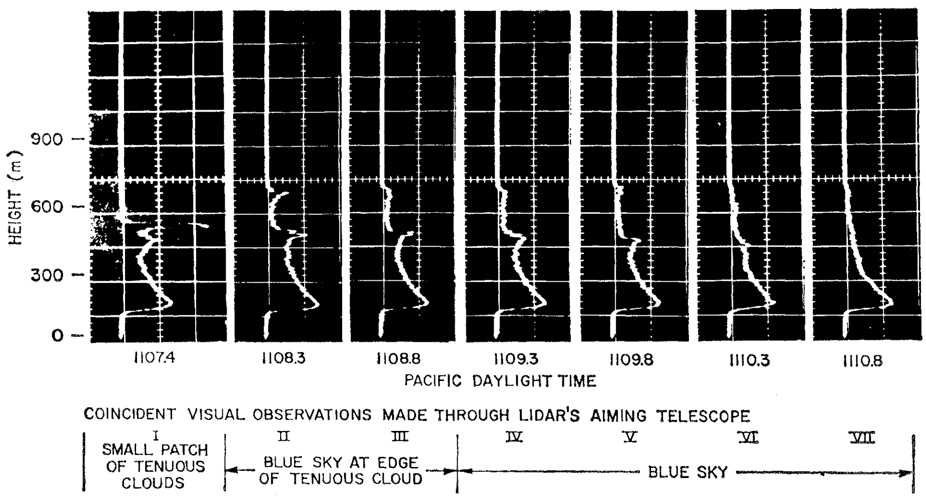

Fig. 5. Dissipating low stratus cloud, 29 September 1964. Series of vertical lidar observations as layer of low stratus dissipated. Surface visibility, 8 km; clear skies as stratus cleared from west. Coincidental visual observations for comparison.

Table 1. Particulars of lidar equipment.

Component	Specifications: Mark I 1963	Mark II 1963	Mark I 1964
Transmitter			
Laser	3 by 0.25 inch (7.5 by 0.6 cm), 90°, C-axis, ruby crystal; transparent and semireflecting coatings on flat ends	3 by 0.25 inch, 90°, C-axis, ruby crystal; transparent and semireflecting coatings on flat ends	3 by 0.25 inch, 90°, C-axis, ruby crystal; Brewster angle ends, uncoated
Q-switch	Rotating prism	Rotating prism	Uranyl glass (UO_2^{++})
Pulse length	30 nsec	30 nsec	24 nsec
Peak power	5 Mw	5 Mw	10 Mw
Optics	None	Refractor, 4-inch aperture	Refractor, 4-inch aperture
Beam width	0.5°	Approximately 0.03°	Approximately 0.03°
Pulse rate	1 per minute	1 per minute	2 per minute
Receiver			
Photomultiplier	10-stage, RCA type 7326	10-stage, RCA type 7326	14-stage, RCA type 7265
Optics	4-inch aperture aerial-camera objective, adjustable field stop	4-inch aperture aerial-camera objective, adjustable field stop	4-inch aperture aerial-camera objective, adjustable field stop
Beam width	0.07° min. to 0.8° max.	0.07° min. to 0.8° max.	0.07° min. to 0.8° max.
Band-pass	Approximately 20 Å	Approximately 20 Å	Approximately 17 Å
Display	Tektronix 555 dual-beam oscilloscope	Tektronix 555 dual-beam oscilloscope	Tektronix 555 dual-beam oscilloscope

Stratus cloud layer and its dispersion. On the forenoon of 29 September 1964, a similar series of vertical observations were made of a layer of stratus as it broke up and dissipated; Fig. 4*b* is a profile made from them. In addition to demonstrating the potential of lidar as a continuously reading ceilometer, this series has certain interesting features relating to the nature of low stratus. At the instant of making each lidar shot, a visual observation was made through the sighting telescope attached to the instrument, and careful notes were made of the condition of the sky probed by the lidar; Fig. 4*a* portrays this series of visual observations. Comparison of the parts of Fig. 4 shows that on occasion weak echoes were returned by what appeared to be clear blue sky, while on other occasions a discontinuity was present, which was apparently related to the top of the inversion layer. The various types of lidar return are well illustrated by the short series of observations shown in Fig. 5, in which the corresponding visual observations are noted. This series (and others of a similar nature) prompt the belief that it may become possible to relate characteristic variations in lidar returns from clear air to the formation of stratus and possibly of fog. Subtle variations in particle concentrations in the aerosol are not perceptible to the eye because of its line-integrating function, and the transition from clear air to cloud is realized as a discrete step. Lidar, however, can perceive changes taking place in the size and concentration of particles or droplets in the subvisible stages of cloud formation and dissipation.

Cirrus cloud. Quite thin cirrus cloud

was readily detectable with the experimental lidars used, even in daylight, provided the angle of view was high—that is, with minimum path attenuation. Echoes were also returned on occasion by what appeared to be clear blue sky, but at heights at which patches of cirrostratus had been visible a short time earlier, or were present elsewhere in the sky.

Lidar has great potential for making cloud observations. Although the systems used here were prototypes, their performance was reliable and straightforward, and I consider that the promise of lidar in this role may be fairly readily realized. Although single-shot observations have great value, higher pulse-repetition frequencies are most desirable. For all purposes, and particularly for operational applications in meteorology and aviation, immediately available recorded displays are needed, with the capability of developing range : height or height : time sections.

RONALD T. H. COLLIS
Stanford Research Institute, Menlo Park, California

References and Notes

1. M. G. H. Ligda, "Meteorological observations with lidar," *Proc. 1964 World Conf. Radio Meteorol. and 11th Weather Radar Conf.*, Boulder, Colo. (1964), pp. 482–489.
2. R. T. H. Collis and M. G. H. Ligda, *Nature* **203**, 508 (1964); R. T. H. Collis, F. G. Fernald, M. G. H. Ligda, *ibid.*, p. 1274.
3. The experimental lidar program was initiated and directed by M. G. H. Ligda. The equipment, which includes components lent by Lear Siegler Corp., was developed under the direction of R. C. Honey. F. G. Fernald, A. Smith, and G. Davis helped with the observations and data reduction. Work sponsored by Lear Siegler Corp. and ONR.

27 May 1965

Major Urinary Protein Complex of Normal Mice: Origin

Abstract. *Mouse serum contains protein having the same charge density and molecular size as the major urinary protein complex of mice. Mouse liver (but not eight other tissues examined) incorporated amino acids labeled with carbon-14 into the complex in vitro. The degree of incorporation was greater in livers from males than from females, and was intermediate in livers from females treated with testosterone.*

The family of proteins excreted in the urine of normal mice, designated the major urinary protein (MUP) complex, is of particular interest since both the phenotype (*1*) and the quantity excreted (*2*) are under the influence of hormones. The protein complex has a weight-averaged molecular weight of 17,800 (*3*) and migrates in moving-boundary (*3*), paper (*2, 3*), or agar-gel electrophoresis as a prealbumin—that is, it migrates faster than albumin when *p*H is above the isoelectric point of albumin. Furthermore, the complex exhibits electrophoretic heterogeneity: electrophoresis in agar gel at *p*H 5.5 yields three components. A phenotypic classification of inbred strains of mice has been made on the basis of mobilities and relative amounts of these components (*1*). Most strains showed phenotypic differences in MUP complex between males and females; moreover, pooled urine from female mice that had been treated with testosterone showed the electrophoretic pattern characteristic of males of the same strain, while urine from castrated males showed the same pattern as that from normal females (*1*).

Immunochemical studies of the origin of MUP have yielded conflicting results: namely, that it is present in serum and probably originates in the liver (*4*) and that it is not present in serum and originates in the kidney (*5*). We now report immunochemical experiments of which the results are direct evidence that MUP is synthesized by the liver.

Urine from BALB/cAnN male mice was dialyzed exhaustively against distilled water and freeze-dried. The nondialyzable fraction was dissolved in 0.9 percent NaCl at a concentration of 0.02 percent. This solution and samples of BALB/cAnN male serum (undiluted or diluted 1 : 2) were placed in alternate wells of an Ouchterlony plate and allowed to react with rabbit antiserum prepared against BALB/cAnN male urinary protein. A single precipitin line formed and showed a reaction of identity.

These same samples and the same antiserum were used in an immunoelectrophoresis experiment in barbital buffer at *p*H 8.2 (*6*). Precipitin arcs formed by urine and serum occupied the same position, anodal to the arc formed by serum albumin with rabbit antiserum prepared against BALB/cAnN male serum.

Our results, in complete agreement with those of Rümke and Thung (*4*), demonstrate that mouse-serum protein immunochemically similar to the MUP complex also exhibits the same mobility. Further evidence of identity came from the following experiment. The urine and serum samples described and the antiserum prepared against urinary protein were allowed to diffuse in agar from troughs placed normal to one another (*7*). Straight precipitin lines formed. The angle between the precipitin line and the mouse-serum trough averaged 58.2 ± 1.3 deg; that between the precipitin line and the urinary-protein trough, 60.3 ± 0.5 deg (*8*). These results indicate no difference in the diffusion coefficients (*7*).

Thus the MUP present in serum has not only the same charge density but also the same molecular size as excreted MUP. Demonstration of the presence of MUP in serum confirms an earlier suggestion (*3*); however, the work of Rümke and Thung (*4*) and other observations (*9*) show that MUP constitutes only a small portion of the mouse-serum prealbumin.

Organ extracts, prepared by grinding fresh tissue in a Potter-Elvehjem homogenizer with 9 volumes of Locke's solution, were examined by immunodiffusion in Ouchterlony plates and by

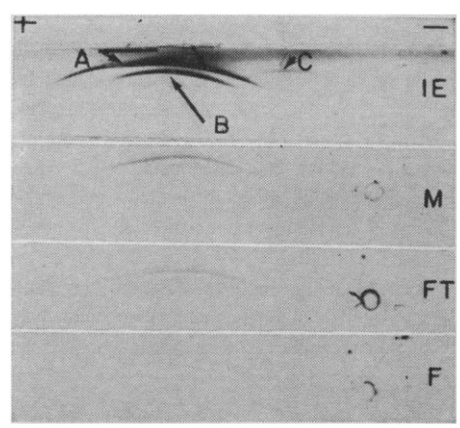

Fig. 1. Incorporation of labeled amino acids into MUP. Arc *A* shows different intensity of labeling, depending on the source of the liver; whether arcs *B* and *C* represent portions of MUP itself is not known, but there was little difference in their degrees of labeling. *IE*, immunoelectrophoretic pattern; *M*, *FT*, and *F*, autoradiographs of culture fluid of liver from individual male, testosterone-treated female, and normal female mice, respectively.